Thermochimica Acta, 145 (1989) 149–163
Elsevier Science Publishers B.V., Amsterdam – Printed in The Netherlands

KINETICS AND REACTION MECHANISMS FOR FORMATION AND DECOMPOSITION OF $Ba_2YCu_3O_x$

AHMED M. GADALLA * and TURI HEGG

Chemical Engineering Dept., Texas A&M Univ., College Station, Texas 77843 (U.S.A.)

(Received 17 August 1988)

ABSTRACT

Thermal curves obtained at constant heating rates of 3, 5 and 10 °C min^{-1} were used to study the kinetics of the solid state reaction of $BaCO_3$, Y_2O_3 and CuO to form $Ba_2YCu_3O_x$ in air. It was evident that three overlapping steps occurred during the formation. After complete formation on cooling, and then on further heating, three reactions occurred. The last three correspond to reactions with partial melting.

From the position of the thermal peaks obtained using different heating rates, Reich's and Kissinger's techniques were used to establish the activation energies for the above reactions. Based on weight loss and using Coats and Redfern's and Šatava and Škvàra's techniques during heating, the activation energy for the six reactions were determined and the mechanisms fitting the results were determined.

INTRODUCTION

Thermogravimetry (TG) and differential thermal analysis (DTA) can be used to study thermal decomposition reactions. The dynamic method, which is the determination of the degree of transformation as a function of time during a linear increase of temperature, has the advantage, compared to the isothermal or static method, that the kinetic parameters can be calculated over an entire temperature range in a continuous manner and fewer samples are required.

Classical chemical reaction kinetics has mainly been concerned with homogeneous reactions and terms such as reaction order and frequency factor are generally meaningless when applied to heterogeneous reactions. In limited cases, only when the reaction order is 0, 1/2, 2/3 or 1, the equations have theoretical significance. This paper reviews methods for dealing with the kinetics and the reaction mechanisms for the superconducting $Ba_2YCu_3O_x$ (213) as described by Gadalla [1–4].

* Author to whom all correspondence should be addressed.

0040-6031/89/$03.50

Simultaneous TG, DTG, and DTA curves for the 213 compound obtained at different heating rates were used to establish the reaction mechanism and the kinetic parameters.

THEORY

Assuming that the reaction is controlled by an activated process, then the kinetic equation could be written in the general form [1,2,4]

$$\beta \frac{\partial \alpha}{\partial T} = Af(\alpha) \exp\left(-\frac{E}{RT}\right) \tag{1}$$

Values of $f(\alpha)$ for possible mechanisms are shown in Table 1.

$$\ln\left(\beta \frac{\partial \alpha}{\partial T}\right) = \ln(Af(\alpha)) - \frac{E}{RT} \tag{2}$$

If $f(\alpha)$ is unknown, Caroll and Manche [6] recommended plotting $\ln(\beta\ \partial\alpha/\partial T)$ versus $1/T$ at a fixed value of α obtained from a series of TG curves carried out at different heating rates. The slope of the straight line obtained is equal to $-E/R$, so the activation energy can be evaluated.

In the presence of consecutive reactions or mechanisms, Carroll and Manche's technique will yield inaccurate results [1,2,4]. The results are also sensitive to slight variation in the slope $\partial\alpha/\partial T$.

The above methods depend on determining the first derivative and are thus known as differential methods. Integral methods can be deduced by rearranging eqn. (1) and integrating

$$g(\alpha) = \frac{A}{\beta} \int_{T_0}^{T} \exp\left(-\frac{E}{RT}\right) \partial T \tag{3}$$

where $g(\alpha) = \int_0^\alpha \partial\alpha/f(\alpha)$. These values are shown for the various possible mechanisms in Table 1.

To find the values of $g(\alpha)$, Reich [7] expressed the exponential part (roughly) in terms of the maximum reaction rate temperature (T_m) read from the DTG curve. This assumption is valid if the reaction occurs over a narrow temperature range. The activation energy can be calculated from Reich's equation using the results obtained at two different heating rates

$$E = \frac{2.303R \log\left[(\beta_2/\beta_1)(T_1/T_2)^2\right]}{(1/T_1) - (1/T_2)} \tag{4}$$

Kissinger [8] used DTA to evaluate the activation energy based on a power-law kinetic equation. Since T_m cannot be read from the DTA curve, he used the peak temperature T_p instead of T_m. Accurate results can thus be obtained if T_p is close to T_m

$$\ln\left(\frac{T_p^2}{\beta}\right) = \ln\left(\frac{E}{R}\right) - \ln A + \frac{E}{RT_p} \tag{5}$$

TABLE 1

Kinetics of heterogeneous solid state reactions [5]

Rate controlling mechanism	Symbol	$f(\alpha)$	$g(\alpha) = \int_0^\alpha d\alpha / f(\alpha) = kt$
Nucleation and nuclei growth			
Random Nucleation			
One nucleus on each particle (Mampel unimolecular law)	F_1	$1-\alpha$	$-\ln(1-\alpha)$
Avrami – Erofeev Nuclei Growth			
Prout–Thompkins branching nuclei	A_1	$\alpha(1-\alpha)$	$\ln[\alpha(1-\alpha)]$
Two-dimensional growth	A_2	$2(1-\alpha)[-\ln(1-\alpha)]^{1/2}$	$[-\ln(1-\alpha)]^{1/2}$
Three-dimensional growth	A_3	$3(1-\alpha)[-\ln(1-\alpha)]^{2/3}$	$[-\ln(1-\alpha)]^{1/3}$
Diffusion			
Parabolic law (one-dimensional diffusion)	D_1	α^{-1}	$\alpha^2/2$
Valensi two-dimensional diffusion (cylinder with no volume change)	D_2	$[-\ln(1-\alpha)]^{-1}$	$(1-\alpha)\ln(1-\alpha)+\alpha$
Three-dimensional diffusion (spherical symmetry, Jander's eqn.)	D_3	$(1-\alpha)^{2/3}[1-(1-\alpha)^{1/3}]^{-1}$	$3/2[1-(1-\alpha)^{1/3}]^2$
Three-dimensional diffusion (Brounshtein–Ginstling's eqn.)	D_4	$[(1-\alpha)^{-1/3}-1]^{-1}$	$3/2[1-(2/3)\alpha-(1-\alpha)^{2/3}]$
Phase boundary movement			
One-dimensional movement (zero order)	R_1	const.	α
Two-dimensional movement (cylindrical symmetry)	R_2	$(1-\alpha)^{1/2}$	$2[1-(1-\alpha)^{1/2}]$
Three-dimensional movement (spherical symmetry)	R_3	$(1-\alpha)^{2/3}$	$3[1-(1-\alpha)^{1/3}]$
Power law		$(1-\alpha)^n$	$[1-(1-\alpha)^{1-n}]/(1-n)$

In addition to the assumption that the activation energy and pre-exponential factor are constants, methods based on the maximum reaction rate temperature (Reich's and Kissinger's) give accurate results only if the reactions take place within the range of 0.9–1.1 T_m. The above mentioned methods can neither establish the operating mechanisms nor differentiate between overlapping mechanisms or reactions.

Coats and Redfern's approximation [9] gives accurate results. Although their initial equations were based on a power-law kinetic equation, their equations could be modified and generalized to suit heterogeneous reactions

$$\log\left(\frac{g(\alpha)}{T^2}\right) = \log\left(\frac{AR}{E\beta}\right) - \frac{E}{2.3RT} \tag{6}$$

When plotting $\log(g(\alpha)/T^2)$ versus $1/T$ for all possible mechanisms, the rate controlling mechanism will give a straight line. The activation energy and the pre-exponential factor can be evaluated from the slope and the intercept, respectively.

Equation (3) can be integrated and written in the form

$$g(\alpha) = \frac{AE}{R\beta} p(x) \tag{7}$$

where

$$p(x) = \frac{e^{-x}}{x} - \int_x^\infty \frac{e^{-u}}{u}\, du$$

$$= \left(\frac{1!}{x^2} - \frac{2!}{x^3}\right) e^{-x} \tag{8}$$

and where $x = E/RT$ and $p(x)$ is a function depending on both temperature and activation energy [10,11]. Šatava and Škvàra [12] plotted $p(x)$ versus T for various activation energies and tabulated the values of $g(\alpha)$ for various mechanisms. They demonstrated that

$$\log[g(\alpha)] - \log[p(x)] = \log\left(\frac{AE}{R\beta}\right) = \text{constant} \tag{9}$$

Plots of $\log[g(\alpha)]$ versus T are made for all possible mechanisms using the same scale as the temperature axis of the $\log[p(x)]$ charts. The curves are then shifted along the $\log[p(x)]$ chart's ordinate until one of the $\log[g(\alpha)]$ curves fits one of the $\log[p(x)]$ curves. From this, the activation energy and the rate controlling mechanism can be established.

To explain why the results over a limited temperature range can fit more than one mechanism, reference should be made to Table 1. It can be seen that $\log[g(\alpha)_{D_3}] = 2\log[g(\alpha)_{R_3}] + \text{constant}$ and $\log[g(\alpha)_{A_3}] = n\log[g(\alpha)_{A_2}]$. This indicates that both R_3 and D_3 will give straight lines with different slopes and the activation energy for D_3 will be twice the calculated value for R_3. Similarly if one of the Avrami–Erofeev mechanisms

operate, A_2 and A_3 will give straight lines with different slopes. Further, it is reported [1,2,4] that D_2 and R_2 are related by the equation

$$\ln(1-\alpha)[\ln(1-\alpha)+\alpha] = 1.89 \ln\left[1-(1-\alpha)^{1/2}\right] + 0.4$$

and D_4 and R_3 by

$$\ln\left[1-\tfrac{2}{3}\alpha-(1-\alpha)^{2/3}\right] = 1.84 \ln\left[1-(1-\alpha)^{1/3}\right] - 0.46$$

These equations indicate that differentiation between D_3, D_4 and R_3 or D_2 and R_2 is difficult. Another difficulty is that the values of $g(\alpha)$ for nucleation mechanisms are much smaller than others leading to straight line fits. This may lead to the wrong conclusion that these mechanisms are the controlling steps [1,2,4].

To overcome the above difficulties, Gadalla [1,2,4] recommended using techniques based on Kissinger's, Reich's or Carroll and Manche's equations for determining the average activation energies as a guide to select the operating mechanism(s).

EXPERIMENTAL TECHNIQUES

$BaCO_3$ (Fischer graded ACS), Y_2O_3 (Æsar graded 99.9% and CuO (Alfa graded ACS), in amounts corresponding to the stoichiometric composition of the 213 compound, were mixed together in an agate mortar. A powder sample of 120 mg was heated in a Netzsch STA 409 using heating rates of 3, 5 and 10 °C min^{-1} to obtain DTA, TG and DTG simultaneously. Burned kaolin was selected as the reference material and crucibles of 99.5% purity alumina supplied by Netzsch were used in this study.

To determine the intermediate phases appearing during the formation of the 213 compound, the constituents were mixed, fired at different temperatures for different periods and examined by X-ray diffraction. The patterns obtained were compared with those for the constituents as well as with those for the binary and ternary compounds reported to exist in the $BaO–Y_2O_3–Cu–O$ system.

RESULTS AND DISCUSSION

Thermal curves obtained for the formation of the 213 compound using $BaCO_3$, Y_2O_3 and CuO in stagnant air were used to study the kinetics of the solid state reactions. Figure 1 shows the first and second heating curve of the 213 compound with a reproducible cooling curve obtained after complete formation of the 213 compound using a heating rate of 5 °C min^{-1}. The peak at around 800 °C on the first heating curve corresponds to a phase

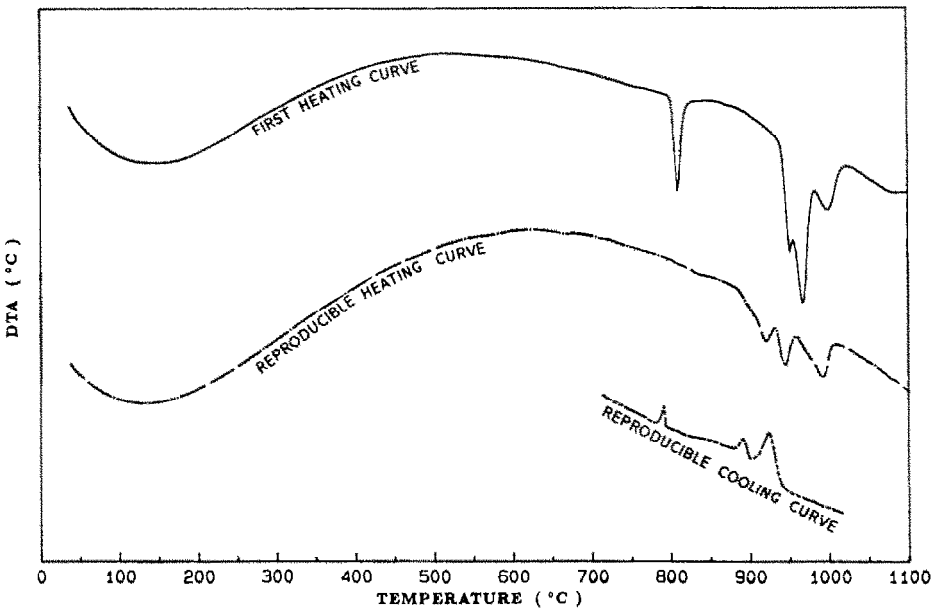

Fig. 1. DTA curves for $BaCO_3$, Y_2O_3 and CuO in the stoichiometric ratio to form the 213 compound.

transition of the $BaCO_3$ from rhombic to hexagonal [13–15]. The hexagonal to cubic transition expected to occur at 980 °C [13–15], occurred at a slightly lower temperature and was accompanied by loss in weight, indicating that during this rearrangement, the crystals were active and the solid state reaction started [16]. After cooling to room temperature and heating using the same rate, the transition of the $BaCO_3$ at around 800 °C was absent confirming the complete consumption of $BaCO_3$. The second heating and cooling curve shows three reversible reactions, which do not correspond to the endothermic peaks obtained in the first run. Accordingly six steps are expected to occur during the formation and decomposition of the 213 compound.

To understand the intermediate steps of the 213 formation, samples were reacted at 800, 850, 900 and 950 °C with soaking periods of 2, 4 and 6 hours. The reacted samples were analyzed by X-ray diffraction. It was evident that $BaCuO_2$ and BaY_2CuO_5 (121) were formed as intermediate compounds before the 213 compound was formed. X-ray diffraction was done without using an internal standard and accordingly the results can be used only qualitatively and not quantitatively. However, the amount of $BaCO_3$ was found to decrease and disappear quickly. $BaCuO_2$ and 121 increased, reached a maximum and disappeared. The latter is what is known as the green phase. These results were confirmed by Keating et al. [17], who studied the heat treatment of spray dried powders between 625 and 975 °C. Their results show a maximum quantity for $BaCuO_2$ at 775 °C and a

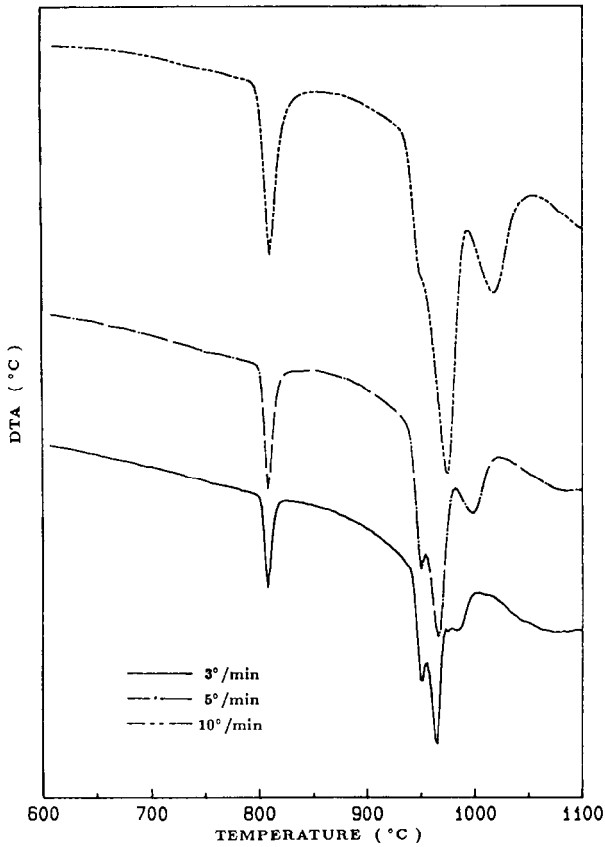

Fig. 2. DTA curves for the formation of the 213 compound in air using heating rates of 3, 5 and 10 °C min^{-1}.

maximum quantity for 121 at 875 °C. The following reactions are thus suggested to represent the intermediate reactions

$$BaCO_3 + CuO \rightarrow BaCuO_2 + CO_2$$

$$Y_2O_3 + BaCuO_2 \rightarrow BaY_2CuO_5$$

$$BaY_2CuO_5 + 3BaCuO_2 + 2CuO \rightarrow 2Ba_2YCu_3O_x$$

This suggests three irreversible reactions occur during formation of the 213 compound. To study the kinetics of these solid state reactions, three heating rates were selected.

Figure 2 shows the DTA curves for 3, 5 and 10 °C min^{-1} obtained for the mixture of $BaCO_3$, Y_2O_3 and CuO in air and it was evident that three overlapping steps occurred during the formation of the 213 compound. The TG curves are shown in Fig. 3 and the DTG curves in Fig. 4. The activation energy was calculated based on the maximum reaction rate temperature (T_m) as it occurred in the DTG curves.

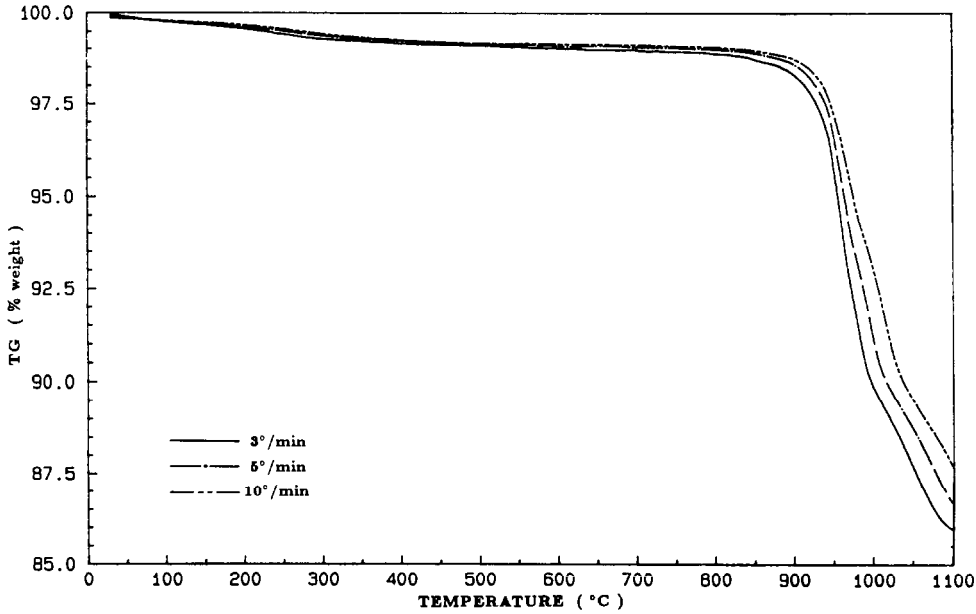

Fig. 3. TG curves for the formation of the 213 compound in air using heating rates of 3, 5 and 10 °C min^{-1}.

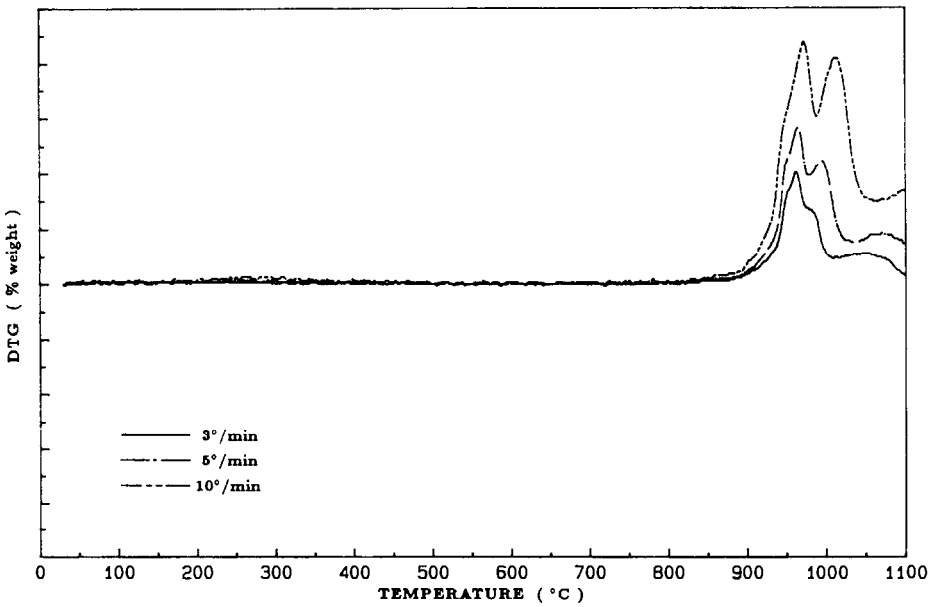

Fig. 4. DTG curves for the formation of the 213 compound in air using heating rates of 3, 5 and 10 °C min^{-1}.

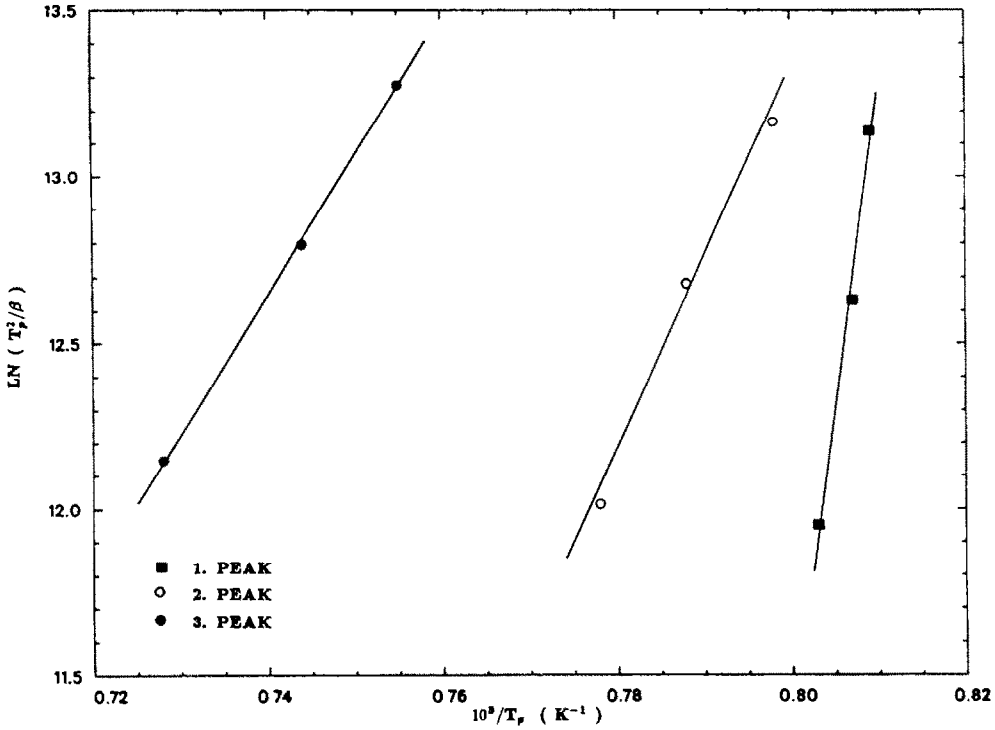

Fig. 5. Determination of the activation energy using Kissinger's method.

To perform Kissinger's technique, $\ln(T_m^2/\beta)$ was plotted against $1/T$ (eqn. (5)) for each step (see Fig. 5). The slope of the straight lines is E/R. The calculated activation energies and the pre-exponential factors are given in Table 2.

Reich's equation (eqn. (4)) was then used to obtain the activation energy for each pair of heating rates. Average values for each step were calculated and are also given in Table 2.

To apply Coats and Redfern's technique, data points from the TG curves were used to calculate $\log[g(\alpha)/T^2]$ for each possible controlling mecha-

TABLE 2

Results from Kissinger's and Reich's methods

Reaction	Kissinger		Reich $E_{avg.}$ (kcal mol^{-1})
	E (kcal mol^{-1})	A (min^{-1})	
1. peak	351	6.2×10^{61}	391
2. peak	116	1.5×10^{19}	115
3. peak	81	2.0×10^{12}	81

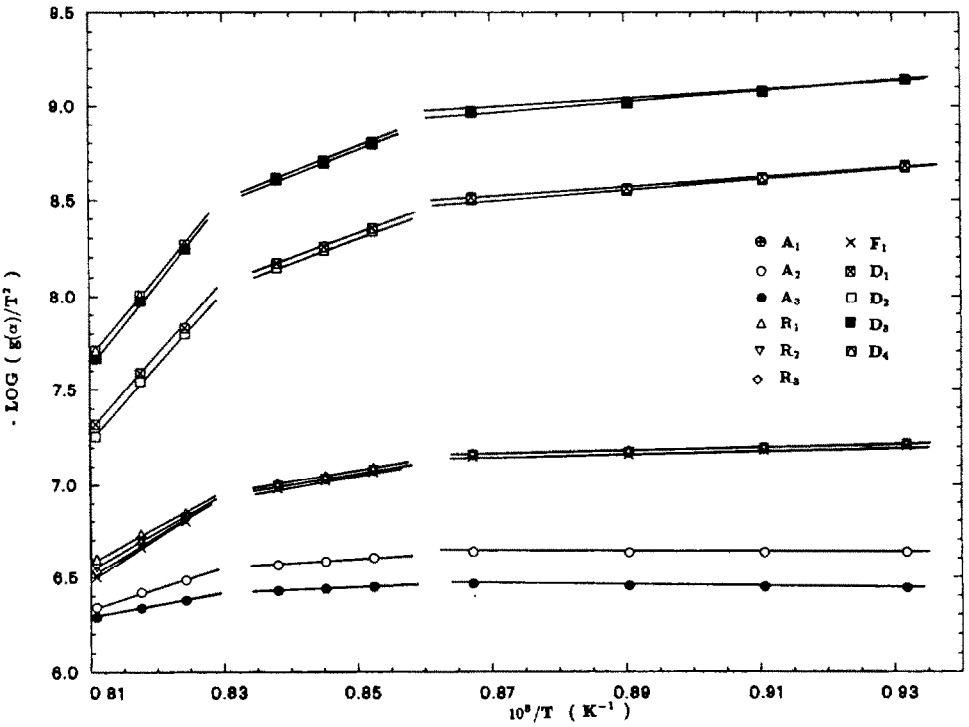

Fig. 6. Variation of $\log[g(\alpha)/T^2]$ with $1/T$ for various mechanisms for steps 1–3 using a heating rate of 3°CC min^{-1}.

nism from 800°C to about 1150°C. These were plotted against $1/T$. Such curves are shown in Figs. 6 and 7 when a heating rate of 3°C min^{-1} was used. Similar curves were obtained for the other heating rates. According to eqn. (6), the best straight line fitting the points determines the mechanism and fixes E and A. From Figs. 6 and 7, it was evident that six overlapping steps occurred during the formation of the 213 compound and their temperature ranges are given in Table 3. It was also observed that more than one straight line can fit the results. As explained above, straight lines with high correlation coefficients and low standard deviations were selected to represent the possible mechanisms. The corresponding kinetic parameters were calculated and are shown in Table 4 separated by "or".

To use Šatava and Škvàra's technique, charts showing the variation of log $p(x)$ versus T were constructed for various activation energies. Values of log $g(\alpha)$ for the possible controlling mechanisms (Table 1) were calculated using the data points from the TG curves and plotted against T using the same T-scale as the log $p(x)$ charts. Figures 8 and 9 show the possible log $g(\alpha)$ curves obtained using a heating rate of 3°C min^{-1}. According to eqn. (9), the curve for $g(\alpha)$ which coincides with a $p(x)$ curve determines the mechanism and fixes the activation energy. From Figs. 8 and 9, it was

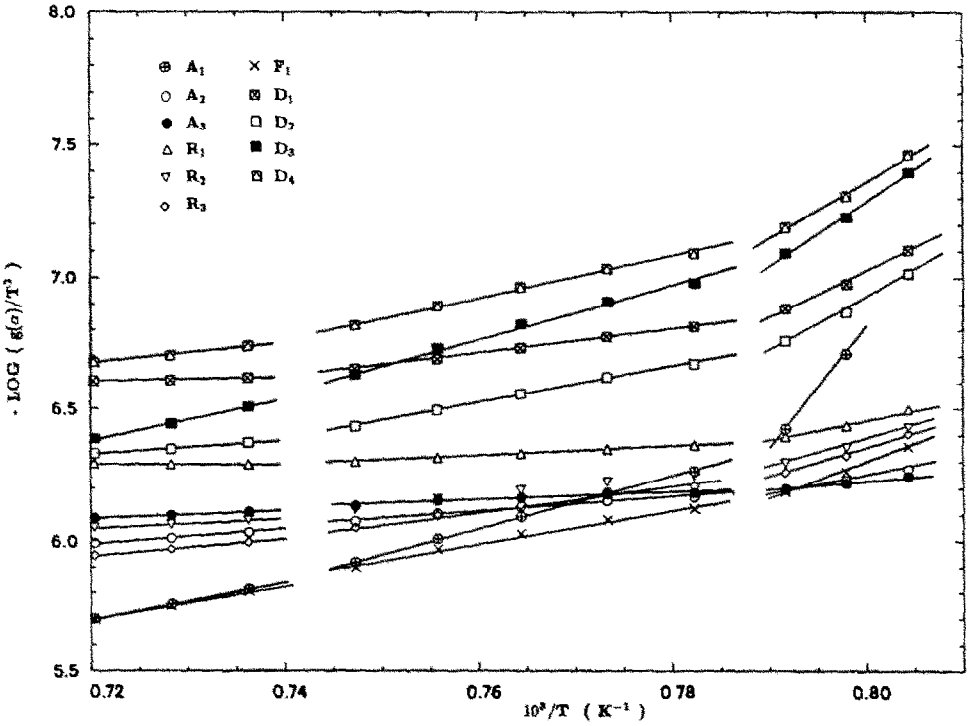

Fig. 7. Variation of $\log[g(\alpha)/T^2]$ with $1/T$ for various mechanisms for steps 4–6 using a heating rate of 3° C min^{-1}.

evident that six overlapping steps occurred as already mentioned under Coats and Redfern's method. When more than one $g(\alpha)$ curve coincided with $p(x)$ curves, the corresponding mechanisms and their activation energies are presented in Table 4 separated by "or". The pre-exponential factors were calculated by use of Coats and Redfern's equation (eqn. (6)).

It was noted that when Coats and Redfern's or Šatava and Škvàra's techniques were applied for the same reaction, the activation energy and the

TABLE 3

Temperature ranges for the six steps

Step	Temperature range (° C)		
	3° C min^{-1}	5° C min^{-1}	10° C min^{-1}
1	800– 890	800– 895	800– 895
2	890– 930	895– 935	895– 930
3	930– 970	935– 965	930– 975
4	970– 990	965–1010	975–1025
5	990–1075	1010–1080	1025–1105
6	1075–1115	1080–1115	1105–1175

TABLE 4

Possible controlling mechanisms and kinetic parameters for the formation and decomposition of the 213 compound

Step	Coats and Redfern			Šatava and Skvàra	
	Mechanism	E (kcal mol^{-1})	A (min^{-1})	Mechanism	E (kcal mol^{-1})
1	D_3	10.6	2.93×10^{-3}	D_3	13.3
	or D_4	10.5	2.67×10^{-3}	or D_4	12.7
	or D_2	10.4	7.64×10^{-3}	or D_2	12.0
2	D_1	63.6	8.99×10^{8}	D_1	68.0
	or D_2	64.9	1.73×10^{9}	or D_2	69.3
	or D_3	66.3	1.13×10^{9}	or D_3	70.0
	or D_4	65.4	7.22×10^{8}	or D_4	70.0
3	D_1	171.7	4.37×10^{30}		
	or D_2	181.5	3.74×10^{32}		
	or D_3	192.2	1.65×10^{34}		
	or D_4	185.0	6.24×10^{32}		
4	D_3	103.6	5.23×10^{16}	D_3	122.7
	or D_4	94.1	5.69×10^{14}	or D_4	112.7
	or D_2	89.3	1.91×10^{14}	or D_2	105.3
5	D_2	28.5	1.15×10^{3}	D_2	53.3
	or D_4	32.4	2.65×10^{3}	or D_4	58.7

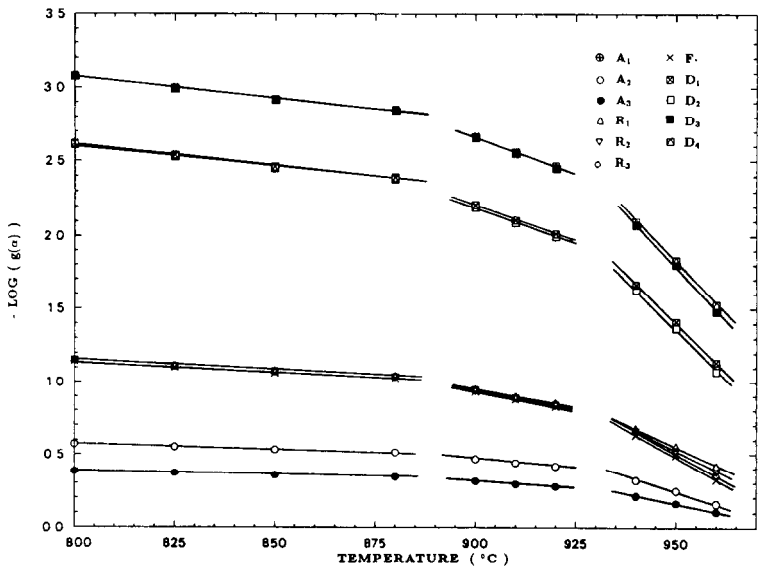

Fig. 8. Variation of log $g(\alpha)$ with temperature for various mechanisms for steps 1–3 using a heating rate of 3° C min^{-1}.

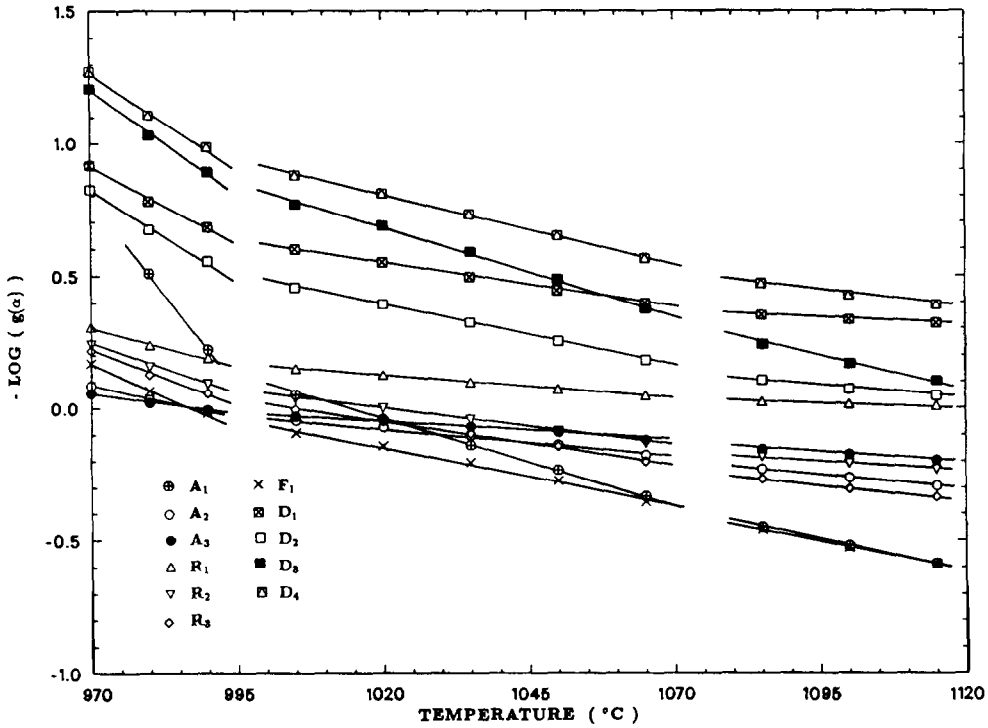

Fig. 9. Variation of log $g(\alpha)$ with temperature for various mechanisms for steps 4–6 using a heating rate of 3°C min^{-1}.

pre-exponential factor decreased with increasing heating rates. The values indicated in Table 4 represent the arithmetic average obtained using the heating rates of 3, 5 and 10°C min^{-1}. Gadalla [4] concluded that with increasing heating rate, the corresponding decrease of the pre-exponential factor tries to compensate the change in the activation energy with increased heat flux to give slight changes in the rate constant.

Because, in this study, the DTA and the TG curves gave a different number of steps, Gadalla's method [1–4] of using values obtained from techniques based on Kissinger's, Reich's or Carroll and Manche's equations for determining the average activation energies as a guide in order to differentiate between the possible mechanisms cannot be used. In this study, values obtained using Šatava and Škvàra's technique were used as a guide to differentiate between the best possible mechanisms.

CONCLUSIONS

The high temperature superconductor, the 213 compound, was found to form and decompose through six overlapping steps. The first three steps

produce the intermediate phases of $BaCuO_2$ and BaY_2CuO_5 before the 213 compound is formed. The last three steps are reversible and correspond to reactions with partial melting. All reactions are found to be diffusion controlled.

LIST OF SYMBOLS

A	pre-exponential factor for Arrhenius equation (min^{-1})
E	activation energy (kcal mol^{-1})
$g(\alpha)$	$\int_0^\alpha \partial\alpha/f(\alpha)$
k	rate constant (min^{-1})
m_0	mass at beginning of step (mg)
m_T	mass at temperature T (mg)
m_v	mass at end of step (mg)
$p(x)$	$(e^{-x}/x) - \int_x^\infty e^{-u}/u \, du$
R	1.987 cal mol^{-1} K^{-1}, universal gas constant
t	time (min)
T	temperature (K)
T_m	maximum reaction rate temperature from DTG curve (K)
T_0	temperature at beginning of step (K)
T_p	peak temperature from DTA curve (K)
x	E/RT
α	$(m_0 - m_T)(m_0 - m_v)$, decomposed fraction
β	$\partial T/\partial t$, heating rate (°C min^{-1})

ACKNOWLEDGMENT

The authors would like to express their thanks to the National Science Foundation, Grant#MSM-8717554 and to the Available University Funds provided by the Board of Regents.

REFERENCES

1 A.M. Gadalla, Int. J. Chem. Kin., 16 (1984) 655.
2 A.M. Gadalla, Thermochim. Acta, 74 (1984) 255.
3 A.M. Gadalla, Int. J. Chem. Kin., 16 (1984) 1471.
4 A.M. Gadalla, Thermochim. Acta, 95 (1985) 179.
5 A. Blažek, Thermal Analysis, Van Nostrand Reinhold, London, 1973, p. 64.
6 B. Carroll and E.P. Manche, Thermochim. Acta, 3 (1972) 449.
7 L. Reich, J. Polym. Sci., 2 (1964) 621.
8 H.E. Kissinger, J. Res. Nat. Bur. Stand., 57 (1956) 217.
9 A.W. Coats and J.P. Redfern, Nature (London), 201 (1064) 68.

10 C.D. Doyle, J. Appl. Polym. Sci., 5 (1961) 285.
11 J. Zsakó, J. Phys. Chem., 72 (1968) 2406.
12 V. Šatava and R. Škvàra, J. Am. Ceram. Soc., 52 (1969) 591.
13 R.H. Perry, Perry's Chemical Engineers' Handbook, McGraw–Hill, New York, 1984, p. 3–8.
14 R.C. Weast and M.J. Astle, CRC Handbook of Chemistry and Physics, CRC Press, Boca Raton, FL, 1984, p. B-72.
15 G. Liptay, Atlas of Thermoanalytical Curves, Heyden and Son, London, 1975, p. 286.
16 A.M. Gadalla and T. Hegg, in C.G. Burnham and R.D. Kane (Eds.), Proc. World Congress on Superconductivity, Progress in High Temperature Superconductivity, Vol. 8, World Scientific, Singapore, 1988, p. 409.
17 S.J. Keating, I.W. Chen and T.Y. Tien, Adv. Ceram. Mater., in press.